Hindawi
Advances in Materials Science and Engineering
Volume 2022, Article ID 5958896, 18 pages
https://doi.org/10.1155/2022/5958896

Research Article

Study of the Effect of Grouting Material Strength on Semiflexible Pavement Material

Qingguo Yang,[1] **Ying Li**,[1] **Hua Zou**,[2] **Long Feng**,[2] **Nan Ru**,[1] **Lin Gan**,[1] **Jiyun Zhang**,[2] **Jiansong Liu**,[2] **and Chengyang Wang**[2]

[1]*School of Civil Engineering, Chongqing Jiaotong University, Chongqing 400074, China*
[2]*China Railway 24th Bureau Group Southwest Construction Co. Ltd, Sichuan 610052, China*

Correspondence should be addressed to Ying Li; 622200030015@mails.cqjtu.edu.cn

Received 21 June 2022; Revised 8 August 2022; Accepted 6 October 2022; Published 1 November 2022

Academic Editor: Giorgio Pia

In this study, cement mortars with different strengths are poured into the large void matrix asphalt macadam material as a semiflexible pavement (SFP) material and the experimental research is carried out. The current research on SFP is mainly focused on the performance of grouting materials and the influence of grouting matrix materials on the overall mechanical properties of SFP and road performance. However, there are some flaws in the study of the influence of grouting material strength on the performance of SFP materials: the difference between the strengths of the selected grouting materials is relatively small, and in some studies, the chosen grouting material strength is low, which leads to insignificant improvements of SFP material performance; besides, the research indicators are also not very comprehensive. In this study, cement grouting asphalt macadam materials are selected as the research object to examine the effect of grouting material strength on the mechanical properties and road performance of SFP materials. Grouting materials with strengths of 19.8 MPa, 30.7 MPa, and 40.2 MPa were poured into the matrix asphalt macadam with a target void ratio of 24% and asphalt content of 2.9% to prepare the corresponding SFP test specimens. The SFP specimens were then subjected to the compressive test, flexural and tensile test, high-temperature stability test, and low-temperature crack resistance test, and the compressive resilient modulus was measured, thereby analyzing the effect of the cement slurry strength on the cement grouting asphalt macadam materials. The results show that when the strength of the cement mortar is 19.8 MPa, 30.7 MPa, and 40.2 MPa, the corresponding SFP material has better mechanical properties. When the strength of the grouting material is 40.2 MPa, the compressive strength of the SFP material is about the same as that of the grouting material. The strength is more than double that of 19.8 MPa and 30.7 MPa, and the flexural tensile strength and elastic modulus also have the above growth laws. The low-temperature crack resistance and high-temperature stability of the SFP material are enhanced with the increase in the strength of the grouting material. When the strength of the grouting material is 40.2 MPa, the mechanical properties and road performance of the SFP material are relatively better. This study provides a reference for strengthening the mechanical properties of SFP materials and boosting the crack resistance of SFP.

1. Introduction

Semiflexible composite pavement is formed by infusing cement slurry into the large void asphalt mixture. Cement grouting asphalt macadam materials, also known as semiflexible pavement (SFP) materials, outperform conventional asphalt concrete materials, and these advantages are attributed to the existence of cement grouting material and matrix asphalt mixture. A convenient, high fluidity, and certain thixotropy green single-component alkali slag grouting material (OAASGM) was prepared by Zhang et al. [1]. The effects of fine sand powder on the setting time, fluidity, rheological properties, and mechanical properties of OAASGM were systematically studied. Experiments show that fine sand powder can effectively prolong the setting time of OAASGM and improve its rheological properties, and the material can be used for SFP materials with high self-grouting saturation and Marshall stability, and is expected to replace cement as a component of (SFP) grouting materials. Yajun and Cahyadi [2] studied the properties such as

microstructure and mechanical strength of silica fume in cement paste and observed that the development of compressive strength in the early stage was not significant, but due to the addition of silica fume, the later stage strength was significantly improved. Fang et al. [3] studied the synergistic effect of polycarboxylate superplasticizer (PCE) and silica fume (SF) on the performance of early high-strength grouting materials (EHSG). The results showed that there is a linear relationship between the flow time of high-fluidity and its dynamic yield stress. Costas [4] studied the effect of polycarboxylate ether-based and sulfonated naphthalene formaldehyde superplasticizers on cement grouting properties and concluded that the use of mineral admixtures can produce high-strength cement useful for tunnel construction grout. Danial Rezazadeh Eidgahee et al. [5] adopt artificial neural network (ANN), genetic programming (GP), and data processing combined group method (GMDH-Combi) for dynamic modulus (E^*) of hot mix asphalt, and the results show that for training the neural network models with correlation coefficients of 0.9821 and 0.9839 for the test were more accurate than the developed models based on GMDH (0.9500 and 0.9503) and GP (0.9493 and 0.9495).

Numerous studies on SFP materials have shown the superior high-temperature stability and low-temperature cracking resistance of SFP materials in comparison with conventional asphalt mixtures. Wang et al. [6] used crack resistance tests to assess the crack resistance of SFP mixtures under different temperature conditions, and the results showed that SFP mixtures have better crack resistance at low temperatures. Hou et al. [7] investigated the mechanical properties and durability of SFP materials and verified that their high-temperature stability, fatigue performance, and water stability were significantly better than those of typical asphalt mixtures. Ding et al. [8] evaluated the performance of semiflexible pavements based on the volumetric parameters of the matrix asphalt mixtures and disclosed that the high-temperature stability and low-temperature stability of semiflexible pavement materials were superior to those of conventional asphalt pavement materials. Zhao and Yang [9] explored the formation of SFP materials based on asphalt concrete skeletons under five distinct gradation types and the low-temperature crack resistance performance of these five skeletons was tested and evaluated. The results displayed that the low-temperature crack resistance capability of the SFP materials based on the continuously graded asphalt concrete skeletons was better than that of other SFP materials.

Some research also has investigated the effect of grouting matrix porosity on the mechanical properties of SFP materials. Yang and Weng [10] evaluated the durability of semiflexible pavement materials by conducting cyclic wheel load tests and discovered that the matrix porosity was the most influential element in determining the durability of SFP material specimens. Husain et al. [11] assessed the effect of the matrix porosity on the durability and compressive strength of SFP materials and revealed that higher matrix porosity contributed to higher strength in SFP materials. Ling et al. [12] investigated the effect of porosity of porous asphalt mixtures on the compressive strain energy density of SFP materials, and the results indicated that the highest strain energy density of SFP materials was achieved when the matrix porosity was 25%. Yang and Weng [10] studied the effects of different factors such as the grouting matrix porosity and the water-cement ratio of the grouting materials on the compressive strength of SFP materials and discovered that the matrix porosity weighed most heavily in determining the compressive strength of SPF materials. Hashem Jahangir et al. [13] conducted an experimental study on the compressive properties of short square-section concrete columns (SRP and SRG composites) restrained by steel fiber reinforced polymer and grouting composites, by comparing the bearing capacity. The ultimate strain was used to evaluate the confinement effect, and the results showed that the general failure modes of the SRP- and SRG-confined concrete columns were the separation of the overlapping surfaces of the fibers and the separation between the core concrete and the composite, respectively.

Moreover, it has also been shown that the type of grouting material also significantly affects the mechanical properties of SFP materials. Koting et al. [14] explored the effect of cement slurry infusion on the properties of SFP mixtures and found that the addition of cement slurry increased the compressive strength, resilient modulus, and spalling resistance of the semiflexible materials. Pei et al. [15] investigated the strength of two SFP materials prepared with high-performance cement slurry and pure cement slurry, respectively, and the results showed that the SFP material prepared with high-performance cement slurry boasted high strength. Zhang et al. [16] prepared the SFP materials by adding cement slurry and cement mortar to the grouting matrix materials, respectively, and then compared the strengths of these two kinds of materials, demonstrating that the SFP material made with cement slurry had better strength, and thus, cement slurry was more suitable for grouting materials. In Afonso et al.'s [17] research, milled glass and waste mud were incorporated into the cement grouts, which then were used to prepare the SFP materials, and the indirect tensile stiffness modulus, the Marshall stability, and the compressive strength of the respective SFP materials were investigated. The results showed that the samples formed by the cement grout with 30% milled glass presented the best mechanical performance. Solouki et al. [18] used traditional cement-based cement and geopolymer-based cement as grouting materials to characterize porous and grouted samples in terms of indirect tensile strength (ITS), indirect tensile strength modulus (ITSM), and moisture sensitivity. Experimental results: it was shown that the control samples grouted with cement-based materials outperformed geopolymer grouting in all respects. Hamzani et al. [19] used waste tire rubber (WTR) powder as an additive and natural zeolite as a cement substitute to study the compressive strength, flexural strength, drying shrinkage, permeability, durability, and stress-strain relationship of semiflexible pavement (SFP). It shows that when the tire rubber powder content is 5% and the zeolite content is 15%, the mechanical properties of SFP are the best. In terms of compressive strength, Hamzani et al. [20] injected cement mortars containing 0%, 5%, 10%, 15%, and 20% natural

zeolite into porous asphalt specimens according to ASTM C670-91a at 14 days of age. The compressive strength test was carried out on the above, and the test results showed that when the natural zeolite content was 15% and the waste tire rubber content was 5%, the compressive strength reached 15.43 MPa. In addition, Hamzani et al. [21] also used materials including waste tire rubber (WTR) and natural zeolite to improve the deformation and fatigue failure of semi-flexible pavement (SFP) under cyclic loading. They carried out a simple support beam with a span length of 30 cm. Fatigue test: the test results show that when the zeolite content is 5%, the performance of maintaining cyclic load is the best.

For the SFP materials, there is also a link between the grouting material strength and the final SFP material strength, provided that the matrix porosity is determined. Cai et al. [22] investigated the uniaxial compressive strength of the SFP material formed by cement slurry with a strength of 6.75 MPa and compared it with porous asphalt concrete (PAC-13). The results showed that the uniaxial compressive strength of the SFP material was close to that of the grouting material, which was much higher than that of PAC-13. However, the effect of the strength of the grouting material on the compressive strength of SFP material was not illustrated in this experiment. Wang et al. [6] investigated the effect of grouting material with a strength of 15.8 MPa on the fatigue performance of the SFP material and compared it with conventional asphalt concrete (AC). The results showed that the fatigue resistance of the SFP material was significantly lower than that of AC under low-temperature and high-stress ratio conditions, but the addition of grouting material was not shown to have a positive effect on the fatigue resistance of the SFP material in this experiment. Cai et al. [23] delved into the effect of grouting material with a strength of 32 MPa and conventional grouting material on the cracking resistance of the SFP material by carrying out a three-point bending test and showed that the grouting material could increase the cracking resistance and deformation ability of the SFP material, while the grouting material with a strength of 32 MPa contributed better to improvements of the SFP material than conventional grouting material. Despite all the preliminary results on the linkage between the grouting material strength and the SFP material in this study, other properties of the material still need to be further investigated. Liang et al. [24] assessed the effects of grouting materials under the maintenance days of 3 d (strength 14.7 MPa) and 28 d on the properties of SFP materials by conducting low-temperature beam bending tests. The increase in grouting material maintenance days was found to improve the bending tensile strength of the SFP material, which was closely related to an increase in the strength of grouting materials, but the exact values of grouting materials at 28 d were not supplied in this experiment. Wang et al. [25] studied the effect of grouting materials with the strengths of 11.20 MPa and 17.74 MPa on the ability of the SFP materials to resist cracking by performing low-temperature beam bending tests, and the results revealed a positive correlation between the crack resistance of the SFP material and the strength of the grouting material. However, the analysis of the low-temperature cracking resistance of the SFP material was incomplete in this experiment as an ideal evaluation method must take into account both strength and deformation. Hong et al. [26] assessed the effect of grouting materials of different strengths (17.4 MPa for S1 and 82.4 MPa for S2) on the freeze-thaw durability of the SFP material and tested the indirect tensile strength of the composites, and the results showed that the SFP-S2 material possessed a higher indirect tensile strength relative to SFP-S1 and the SFP-S2 material showed better resistance to freezing, but in this experiment, the increase in the indirect tensile strength was not identified. Based on the three-point bending fatigue test, Ren et al. [27] explored the effects of two grouting materials with strengths of 12.18 MPa and 35.01 MPa on the fatigue performance of the SFP materials, and the results showed that the fatigue strength of SFP materials increased with the increase in the grouting material strength. Fang et al. [28] examined the effect of grouting materials with strengths of 7.7 MPa and 10.2 MPa on the low-temperature crack resistance of SFP materials, and the results showed that the low-temperature crack resistance of SFP materials increased with the increase in the grouting material strength. Imran Khan and Hartadi Sutanto [29] studied the effect of grouting materials with strengths of 9.57 MPa and 12.36 MPa on the compressive strength of SFP materials, and the results showed that the compressive strength of SFP materials increased with the increase in the strength of grouting materials. In the abovementioned two experiments, however, the effect on the properties of SFP materials was not significant due to the small difference between the strengths of the grout, which needs to be further investigated. Tan et al. [30] assessed the effect of two grouting materials with different strengths (0.82 MPa for A and 0.72 MPa for B) on the crack resistance of the SFP material by the semicircular bending (SCB) test. The results showed that the crack resistance of the SFP mix increased with the increase in the strength of the grouting material, but in this experiment, the strength of the grouting material was low and the influence hence was not obvious. Much remains to be done to study the effect of the grouting material strength on the properties of the SFP material. In a nutshell, the studies mentioned above clarify the relationship between the strength of the grouting material and the mechanical properties of the final SFP material, which is conducive to the design of pavement materials.

The performance of the SFP materials can be improved by injecting grouting materials of different strengths, as indicated above, but there are still some issues that need to be addressed. Cai et al. [22], Wang et al. [6], Cai et al. [23], and other scholars in their studies selected the grouting materials of single strengths, leading to a lack of comparability in the effects of different grouting material strengths on the SFP material performance. The difference between the grouting material strengths chosen by Wang et al. [25], Fang et al. [28], and Imran Khan and Hartadi Sutanto [29] is not significant, and as a result, the improvements in the SFP material performance are not obvious, failing to obtain the substantial change pattern of the grouting material

strength's influence on the performance of SFP materials. Besides, the indicators employed in those studies to assess the influence of grouting material strength on the performance of SFP materials are not very comprehensive. The grouting material selected by Tan et al. [30] is low in strength, and hence, its effect on the performance improvement of the SFP material is obscure. To sum up, the effect of the grouting material strength on the performance of the SFP material necessitates further research.

Given this, this study prepares SFP materials by infusing grouting materials with strengths of 19.8 MPa, 30.7 MPa, and 40.2 MPa into large void matrix asphalt macadam and investigates the effect of the grouting material strength on the SFP materials through various experiments. Since the strength of the selected grouting material has a certain contrast, the strength increases regularly, which is helpful for us to more intuitively observe the substantial change law of the influence of different grouting material strength on the performance of the SFP material. In this study, five indicators are selected to study the improvement of grouting material strength on the performance of SFP materials, such as compressive strength, low-temperature crack resistance, high-temperature stability, flexural tensile performance, and elastic modulus. Compared with previous research, this paper will be more specific and more comprehensive. To determine the appropriate curing period and provide some guidance for selecting the appropriate cement grouting material strength for SFP, the research conclusions will have important reference significance for the performance of semiflexible composite materials and pavement design.

2. Materials and Methods

2.1. Cement Slurry Test Materials and Proportions

2.1.1. Test Raw Materials

(1) Cement. The cement used in this study is P-O42.5R conventional silicate cement produced by Chongqing Lafarge Cement Plant [31, 32]. The quality of the cement is up to standard and can meet the requirements of cement slurry according to the test methods stipulated in Test Specification for Cement and Concrete in Highway Engineering, and the test results are shown in Tables 1–3.

(2) Fine Sand. The fine sand used in this research is the fine sand produced by Taifeng Sand Mining Factory in Dazu District, Chongqing. The selected sand should be clean, hard, wear-resistant, and small in particle size. The screening results are shown in Tables 4 and 5.

(3) Fly Ash. Class I fly ash produced by Henan Hengyuan New Materials Co. Ltd. is used after passing through a 0.6 mm sieve hole. The screening results are shown in Tables 6 and 7.

(4) Admixtures. Two kinds of admixtures were used in the research in this study. One is the UEA expansion agent purchased from Shandong Hongxiang Company. The use of swelling agents ensures good bonding, reduces bleeding, and minimizes shrinkage cracks. The second is the polycarboxylate water-reducing agent purchased from Shanghai Chenqi Environmental Protection Company, which is used to improve the uniformity of cement mortar and achieve the effect of preventing the delamination of sand and mortar in cement mortar, accounting for 1% of cementitious materials.

2.1.2. Determination of the Cement Slurry Mix Ratio.

The recommended dosing of each factor of the cement slurry mix ratio for grouting is derived from a review of the literature [33–36]. The optimal range of water-binder ratio is 0.45–0.55, the range of fly ash admixture is 0.1–0.15, the range of sand-binder ratio is 0.2–0.25, the UEA expansive agent is 0.08, and the polycarboxylate superplasticizer is 0.01. The recommended mix ratios are ① ② ③, and the details are shown in Tables 8 and 9.

2.2. Mix Ratio Design of the Matrix Asphalt Macadam

2.2.1. Raw Materials for Asphalt Macadam

(1) Asphalt. SBS-modified asphalt from Chongjiao Industrial Co. Ltd is tested according to methods in the *Test* Procedure for Asphalt and Asphalt Mixture for Highway Engineering (JTG E20-2011), and this kind of asphalt meets the requirements, as shown in Table 10.

(2) Aggregates. Aggregate is the main body in the matrix asphalt crushed stone, and the performance of the aggregate greatly affects the performance of the final composite material. To make the matrix asphalt macadam meet the requirements of porosity and ensure a reasonable embedded structure, this study adopts the discontinuous gradation to design the matrix asphalt macadam. The limestone produced by Chongqing Yubei Heavy Industry Co. Ltd. is used in this study. The coarse aggregate adopts a single particle size, which is 9.5 mm–13.2 mm, and the fine aggregate is 1.18 mm–2.36 mm. Refer to the "Highway Engineering Aggregate Test Regulations" to determine the aggregate performance indicators. The specific results are shown in Tables 11 and 12.

(3) Slag Powder. The chosen limestone GGBS (ground granulated blast furnace slag) is obtained from Chongjiao Industrial Co. Ltd, and the sieve passing rates are shown in Table 13.

2.2.2. Mix Ratio of Matrix Asphalt Macadam at Target Void Ratio.

At present, the main method for determining the amount of asphalt in common asphalt mixtures is the Marshall method, and the porosity of the asphalt crushed stone material is as high as 20%, which belongs to the skeleton void structure. For the determination of the optimal amount of asphalt for large void matrix asphalt, there are currently related methods such as the Schellenberg asphalt leakage test, the Cantabro Test, the Martens test, and the

Table 1: Cement test indicators.

Indicators	Specific surface area (/kg)	Initial setting time (min)	Final set time (min)	Compressive strength (MPa)		Flexural strength (MPa)	
				7 d	28 d	7 d	28 d
P-O42.5R	315	228	380	37.8	43.2	5.92	6.85

Table 2: Main chemical components of cement.

Fe_2O_3	Al_3O_2	SiO_2	LOI	K_2O	Na_2O	CaO	MgO
2.5	4.3	21.1	3.2	0.5	0	65.9	1.5

Table 3: Main chemical components of cement.

Project	Particle distribution (%)						
	≤1 μm	1~3 μm	3~10 μm	10~30 μm	30~45 μm	45~60 μm	≥60 μm
P.042.5R	17.33	9.57	16.63	25.78	10.38	12.39	7.92

Table 4: Fine sand sieving results.

Max particle size mm	Sieve holes	0.6	0.3	0.15	0.075
0.6	Passing rate	100	48.6	4.4	1.8

Table 5: Physical index of fine sand.

Project	Fineness modulus	Mud content (%)	Bulk density (kg/m^3)	Apparent density (kg/m^3)	Loose bulk density (kg/m^3)
Fine sand	0 804	16	1250	2540	1350

Table 6: Chemical composition of fly ash (%).

Fe_2O_3	Al_3O_2	SiO_2	LOI	K_2O	Na_2O	CaO	MgO
11.55	28.11	53.72	1.05	0.5	0.75	3.54	0.78

Table 7: Fly ash particle size distribution.

Project	Particle distribution (%)						Specific surface area (m^2/kg)
	≤5 μm	5~10 μm	10~20 μm	20~30 μm	30~45 μm	≥45 μm	
Fly ash	19.48	28.54	36.69	6.22	6.22	3.25	325

Table 8: Cement slurry mix ratios.

No.	Cement	Fly ash	Water	Fine sand	Expansive agents	Polycarboxylate superplasticizer	Water-binder ratio	Sand-binder ratio
①	0.8	0.12	0.45	0.2	0.08	0.01	0.45	0.2
②	0.8	0.12	0.45	0.25	0.08	0.01	0.45	0.25
③	0.8	0.12	0.49	0.25	0.08	0.01	0.49	0.25

Table 9: Performance test results.

Numbering	Mobility (s)	Bleeding rate (%)	Compressive strength (MPa)			Flexural strength (MPa)			Shrinkage (1×10^{-6})
			7 d	14 d	28 d	7 d	14 d	28 d	
①	13.21	4.58	8.2	14.1	19.8	2.24	3.66	4.73	3868
②	12.27	2.67	19.1	33.6	40.2	4.61	5.87	9.13	2644
③	12.54	3.81	12.7	25.2	30.7	3.42	5.22	7.25	3186

Table 10: Test results of SBS-modified asphalt performance.

Test indicators		Unit	Test results	Specification requirements	Test method
Needle penetration (25°C, 100 g, 5 s)		0.1 mm	72	60–80	T0604-2011
Ductility (5°C, 5 cm/min)		cm	56	≥30	T0605-2011
Softening point		°C	76	≥55	T0606-2011
Flash point		°C	310	≥230	T0611-2011
Solubility (trichloroethylene)		%	99.8	≥99	T0607-2011
Kinematic viscosity (135°C)		Pa-s	2.1	≤3.0	T0619-2011
Segregation (48 h softening point difference)		°C	1.9	≤2.5	T0661-2011
Elastic recovery (25°C)		%	87	≥65	T0662-2000
Relative density of asphalt		g/cm³	1.030	Real testing	T0603-2011
TFOT of aging residue (163°C, 5 h)	Quality changes	%	0.14	≤±1.0	T0609-2011
	Needle penetration ratio	%	77.6	≥60	T0604-2011
	Ductility	cm	42	≥20	T0605-2011

Table 11: Limestone coarse aggregate performance index.

Technical index	Unit	Test results	Requirements	Experiment method
Apparent density	g/cm³	2.737	≥2.60	T0304—2005
Crush value	%	19.1	≤26	T0316—2005
Los Angeles wear value	%	18.6	≤28	T0317—2005
Sturdiness	%	3.5	≤12	T0314—2000
Water absorption	%	0.45	≤2.0	T0304—2005
Needle-like particle content	%	8.2	≤12	T0312—2005

Table 12: Limestone fine aggregate performance index.

Technical index	Unit	Test results	Requirements	Experiment method
Apparent density	g/cm³	2.732	≥2.50	T0328—2005
Water absorption	%	0.58	≤2.0	T0328—2005
Sand equivalent	%	76.8	≥60	T0334—2005
Sturdiness	%	15.4	≥12	T0340—2005

Table 13: Slag powder sieving passing rate.

Sieve hole size (mm)	0.15	0.075
Passing rate (%)	100	91

calculation of the asphalt film thickness. In view of the lack of research in this area, more reference is made to the research results of other scholars on the optimal amount of asphalt. According to the properties of the SBS-modified asphalt used, the amount of modified asphalt with a target porosity of 24% is set as 2.9%. Then, referring to the research results of Cheng [37], on the optimal asphalt dosage, the larger the target porosity, the greater the optimal asphalt dosage, and the optimal asphalt dosage corresponding to other target porosity is determined. In this study, the target porosity of 24% cement grouting asphalt crushed stone material is selected for research, and the specific gradation and Marshall test results are shown in Tables 14 and 15.

3. Test Specimen Production

3.1. Specimen Forming and Grouting. In this study, cement slurries with strengths of 19.8 MPa, 30.7 MPa, and 40.2 MPa are chosen to be filled into a matrix asphalt macadam with a target void ratio of 24% and asphalt content of 2.9% to form the specimens (Figure 1).

3.1.1. Marshall Specimen Forming. The Marshall specimens are prepared and formed in the following three steps: (1) the matrix asphalt macadam Marshall specimens are prepared by Test Methods of Asphalt and Asphalt Mixtures for Highway Engineering (JTG E20-2011); (2) the cement slurry is grouted on a vibrating table; (3) after grouting, let it stand at room temperature for 24 hours to demold, and then, the test piece is placed in a constant temperature water temperature tank that has reached the specified temperature, and the standard Marshall test piece for 40 minutes is held. The head is placed in a sink or oven to the same temperature. (4) The upper and lower indenters of the Marshall test piece are taken out and the inner surface is cleanly wiped, and a little butter is applied on the guide rod of the lower indenter to make the upper and lower indenters slide freely. The test piece is taken out, it is placed on the lower indenter, the upper indenter is covered, it is installed on the loading equipment, and the test is carried out.

3.1.2. Rutting Specimen Forming. The rutting specimens are prepared and molded in three steps: (1) the matrix asphalt macadam rutting specimens are prepared by Test Methods of Asphalt and Asphalt Mixtures for Highway Engineering (JTG E20-2011); (2) the mixture is mixed on the vibrating table; (3) after the mixture is mixed, the preheated test mold

Table 14: Gradation of matrix asphalt macadam at target void ratio.

No.	Target void ratio (%)	Asphalt content (%)	Slag powder content (%)	1.18 mm to 2.36 mm (%)	9.5 mm to 13.2 mm (%)
	24	2.9	2	9.46	88.54

Table 15: Matrix asphalt crushed Marshall test.

Project	Whetstone ratio (%)	Gross bulk density (g/cm^3)	Porosity (%)	Connected porosity	Stability (kN)	Flow value (0.1 mm)
Matrix asphalt crushed	4.0	2.023	21.5	15.9	9.65	2.33

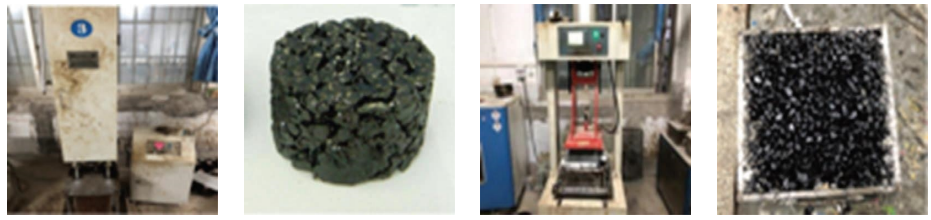

(a) (b) (c) (d)

Figure 1: Formation of the specimen: (a) Marshall compactors. (b) Marshall specimen. (c) The rolling of the matrix asphalt macadam. (d) The formation of the matrix asphalt macadam.

is taken out from the oven and the test mold frame is installed. A piece of plain paper is laid in the test mold, so that the bottom plate and sides of the test mold are separated by paper. After the mixed mixture is slightly mixed with a spatula in the holding tray, it is evenly rotated along the test mold from the side to the middle and placed into the test mold. The middle part is slightly above the four sides, two people cooperate with each other, one person installs the mold, and the other person is responsible for tamping with the preheated small hammer from the edge to the transfer circle, the middle part is higher than the four sides, and all the mixture is put into the test mold; (4) the trial frame is removed, and a preheated small compaction hammer is used to compact it from the edge to the middle, and it is flattened into a convex arc shape; (5) the thermometer is inserted into the loaded mixture, and the mixture is covered with paper to prevent the watch and the temperature from dissipating too quickly and waited until the thermometer shows that the mixture is cooled to the required compaction temperature; (6) for rolling forming, first the rolling wheel is preheated to 100°C. Then, set the trial mold containing the mixture on the platform of the wheel rolling machine, the rolling wheel is gently lowered, the load roller (7) is adjusted to start the rolling wheel, 2 round trips (4 times) are rolled first in one direction to unload, and then the rolling wheel is lifted to remove the load. The test piece is turned 180 degrees and is rolled with the same load until the Marshall standard compactness (1004–1). After compaction and molding, a marker is used to mark the rolling direction on the surface of the test piece; (8) and the test mold containing the compacted test piece is placed at room temperature to cool for 12 hours.

3.1.3. Grouting. After the temperature of the base asphalt crushed stone is less than 40°C, a plate vibrator is used to promote the penetration of the slurry. After the penetration is completed, a rubber scraper is used to scrape off the excess slurry to expose the unevenness of the surface of the asphalt mixture specimen. The test piece is placed together with the template on the vibrating platform, the prepared cement mortar is placed aside, the vibrating table is turned on, and perfusion is performed. The perfusion is horizontally from the low side to the high side, and the longitudinal direction is from the bottom of the slope to the top of the slope. If the perfusion is not smooth, the vibration must be strengthened, and the vibration should be strengthened where the glue flows to avoid solidification on the surface and block the voids of the gravel. During the pouring process, it is necessary to continuously stir the cement mortar, repeatedly drag the test mold with a rubber road rake to make it naturally saturated, and drag the excess mortar on the surface of the test mold to the lack of pulp. When using platform vibration, be sure to vibrate back and forth until the injected mortar is vibrated until it no longer flows downward. Generally, grouting should be performed in the manner of perfusion-vibration-perfusion and repeated at least 3 times to strictly avoid vibration leakage. The grouted specimens were allowed to stand at room temperature for 24 hours. After the slurry was hardened, they were placed in a curing room with a temperature of 20°C ± 3°C and a humidity greater than 90% for 28 days, and then, the physical properties were measured. Then, the specimens are cut into the required size. The grouting process is shown in Figure 2.

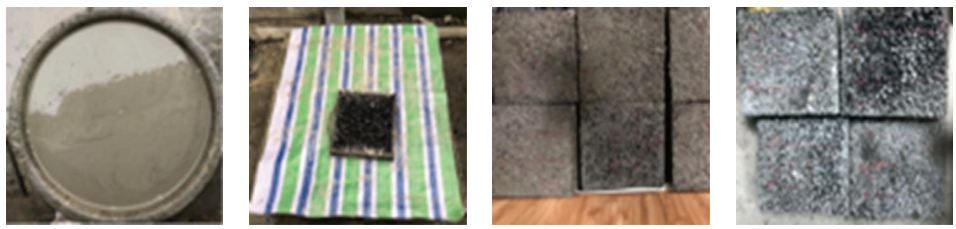

(a) (b) (c) (d)

Figure 2: Grouting and formation of specimens. (a) Prepared cement slurry. (b) Grouting on the vibrating table. (c) Rutting specimens after grouting. (d) Rutting specimens after maintenance.

4. Experimental Methods

4.1. The Compressive Test. The compressive strength test of cement grouting asphalt macadam is carried out by Uniaxial Compression Test Method for Asphalt Mixture (T0714–1993) from Standard Test Methods of Bitumen and Bitumen Mixture for Highway Engineering (JT J 052–2000). The compressive strength test specimens are cut from standard rutting plates obtained from the wheel rolling method and are prisms of 40 mm ± 1.0 mm in length, 40 mm ± 1.0 mm in width, and 80 mm ± 2.0 mm in height. Three specimens of the same composite material are cut at the same age and maintained under standard conditions for 7 d, 14 d, and 28 d and then subjected to uniaxial compression tests at all three ages. The tests were carried out on a compressive machine according to the test protocol.

During the test (Figure 3), the maximum load $_{Pc}$ at the time of damage to the specimen and the damage deformation ΔL at the corresponding maximum load are obtained. The compressive strength of the specimen R_c at the time of damage, the compressive strain ε_c, and the stiffness modulus in compression S_c can be calculated according to the following equations:

$$Rc = \frac{Pc}{(b \times h)}, \tag{1}$$

$$\varepsilon c = \frac{\triangle L}{L}, \tag{2}$$

$$Sc = \frac{Rc}{\varepsilon c}. \tag{3}$$

In the above equation, R_c represents the compressive strength of the specimen (MPa), P_c represents the maximum load (N) of the specimen at the time of damage, b represents the length of the specimen (mm), h represents the width of the test piece (mm), ε_c represents the compressive strain at the damage of the specimen, Δ_L represents the compression deformation of the specimen at the time of damage (mm), L represents the height of the specimen (mm), and S_c represents the stiffness modulus of the specimen in compression (MPa).

4.2. Flexural and Tensile Tests. The flexural and tensile strength test of cement grouting asphalt macadam is carried out by the Bending Test of Asphalt Mixture (T0715-2011) from Test Methods of Asphalt and Asphalt Mixtures for Highway Engineering (JTG E20-2011). The test specimens are also cut from standard rutting plates using the wheel rolling method and are prismatic beams of 250 mm ± 2.0 mm in length, 30 mm ± 2.0 mm in width, and 35 mm ± 2.0 mm in height. Three specimens of the same composite material are cut at the same age and maintained under standard conditions for 7 d, 14 d, and 28 d, and then, the beam bending tests are carried out at three ages. The tests are carried out on a universal testing machine at a controlled temperature of 15°C ± 0.5°C. The specific methods and procedures are in line with the test protocol.

During the test (Figure 4), the maximum load P_B at the time of damage to the specimen and the mid-span deflection d at the time of damage are obtained. The flexural and tensile strength of the specimen R_B at failure and the maximum flexural tensile strain at the bottom of the beam ε_B at the time of failure and the modulus of flexural stiffness S_B at damage can be calculated by the following equations:

$$R_B = \frac{3 \times L \times P_B}{2 \times b_1 \times h_1^2}, \tag{4}$$

$$\varepsilon_B = \frac{6 \times h_1 \times d}{L^2}, \tag{5}$$

$$S_B = \frac{R_B}{\varepsilon_B}. \tag{6}$$

In the above equations, R_B represents the flexural and tensile strength of the specimen at the time of damage (MPa). ε_B represents the maximum flexural tensile strain ($\mu\varepsilon$) at the time of damage to the specimen. S_B represents the modulus of flexural stiffness of the specimen at the damage (MPa), b_1 represents the width of the specimen at mid-span (mm), h_1 represents the height of the specimen at mid-span (mm), L represents the span of the specimen (mm), P_B represents the maximum load (N) of the specimen at the time of damage, and d represents the mid-span deflection of the specimen at the time of damage (mm).

4.3. Resilient Modulus Test. The rebound modulus test of cement grouting asphalt macadam is carried out by the Uniaxial Compression Test of Bituminous Mixtures (Cylinder) (T0713-2000) from Standard Test Methods of

(a) (b)

Figure 3: Compressive test of the specimens. (a) Compressive machine. (b) The compressive test process.

(a) (b)

Figure 4: Flexural and tensile test of the specimen. (a) Universal testing machine. (b) Bending test procedure.

Bitumen and Bitumen Mixture for Highway Engineering (JT J 052–2000). The compressive rebound modulus test specimens are obtained through core drilling from a standard rutting plate using the wheel rolling method and are cylinders of 100 mm ± 2.0 mm in diameter and 100 mm ± 2.0 mm in height. Six specimens of the same composite material are drilled, three for the compressive strength test and three for the compressive resilient modulus test. They are maintained for 28 d under standard conditions and then tested at two temperatures of 15°C and 20°C, respectively. The tests are carried out on the universal material testing machine, and the specific methods and procedures are carried out by the test protocol.

The compressive strength of the cylinder is calculated according to the following equation:

$$R_c = \frac{4P}{\pi d^2}. \tag{7}$$

In the above equation, R_c represents the compressive strength of the specimen (MPa), P represents the maximum load (N) of the specimen at the time of damage, and d represents the specimen's diameter (mm).

The actual compressive strength of the specimen q_i at each level of loading is calculated according to equation (8). The details of q_i and ΔL_i are recorded and plotted on a square grid, and the $q_i - \Delta L_i$ relationship is plotted as smooth continuous curves, which intersect with the coordinate axes to obtain the corrected origin. The compressive strength at the fifth level of loading and the corresponding ΔL_5 are obtained based on the coordinates of this corrected origin. The compressive rebound modulus is calculated according to equation (9).

$$q_i = \frac{4P_i}{\pi d^2}, \tag{8}$$

$$E' = \frac{(q_i \times h)}{\triangle L_5}. \tag{9}$$

In the above equations, q_i represents the compressive strength of the specimen at test loading at each level P_i (MPa), P_i represents the value of the load exerted on the specimen at all levels (N), E' represents the compressive resilient modulus (MPa), q_5 represents the compressive strength (MPa) at the test loading at the fifth level (0.5P), h represents the height of the specimen axis (mm), and ΔL_5 represents the specimen's rebound deformation (mm) at the test loading at the fifth level (0.5P) after origin correction.

4.4. High-Temperature Stability Tests. At present, the indoor methods for evaluating the high-temperature stability of asphalt pavement in our country include Marshall test method (including Marshall stability, flow value, and Marshall modulus), creep test, rutting test, and loop test method, among which the most widely used is the Marshall test law, but it has certain limitations. Research by the University of Nottingham shows that the Marshall test is not a good method to evaluate the permanent deformation resistance of asphalt pavement; the stability and flow value of asphalt mixture designed by the Marshall method have little

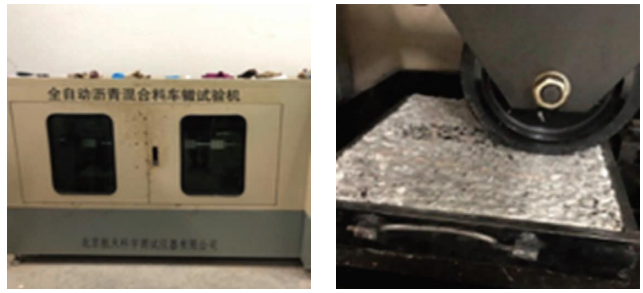

(a) (b)

Figure 5: High-temperature stability test. (a) Rutting tester. (b) Rolling process.

correlation with the actual pavement; our country's "Seventh Five-Year" research project also proved this and further proved that the rutting test has a good correlation with the actual asphalt pavement. Therefore, in view of the simplicity and intuitiveness of the rutting test method and the good correlation with the actual rutting of the road surface, in addition to using the Marshall test method to evaluate its high-temperature stability, this study mainly used the rutting test to test the rutting resistance of semiflexible pavement composites. The high-temperature stability of cement-grouted asphalt aggregates was investigated by Test Method for Rutting of Asphalt Mixture (T0719-2011) from Test Methods of Asphalt and Asphalt Mixtures for Highway Engineering (JTG E20-2011). The test specimen is a rutting plate of 300 mm in length, 300 mm in width, and 50 mm in thickness, to be grouted after rolling to ensure that the cement grouting is dense. After the test piece is formed, it should not be placed at room temperature for less than 12 hours together with the test mold, but it should not be placed at room temperature for more than a week and subjected to rutting tests as shown in Figure 5.

The dynamic stability (DS) is used as an indicator of the rutting resistance of the asphalt mixture. During the test, the recorder automatically records the deformation curve and the temperature of the specimen, while the dynamic stability is the calculated value of the slope of the deformation curve over a certain period, from 45 min to 60 min according to the specification. The amounts of rutting deformation d_1 and d_2 at 45 min (t_1) and 60 min (t_2) are obtained from the deformation curve, which is accurate at 0.01 mm. The test temperature is set to be at 60°C ± 0.5°C, and the wheel load is 0.7 MPa. DS can be calculated according to the following equation:

$$\mathrm{DS} = \left[\frac{(t_2 - t_1) \times N}{(d_2 - d_1)}\right] \times C_1 \times C_2. \quad (10)$$

In the above equation, DS refers to the dynamic stability of the asphalt mix (times/mm), t_1 and t_2 represent the test periods, usually 45 min and 60 min, d_1 represents the amount of deformation (mm) during t_1, d_2 represents the amount of deformation (mm) during t_2, C_1 represents the testing machine type factor, 1.0 for the round-trip mode of operation of the wheel driven by the crank and connecting rod mechanism, C_2 represents the specimen's factor, 1.0 for the 300 mm wide laboratory specimen, and N represents the rolling speed of the test wheel in its round trip, usually 42 times/min.

4.5. Low-Temperature Crack Resistance Test. Pavement crack resistance and material low-temperature performance indicators have always been important research contents in the international road academic community. The SHRP program in the United States includes the study of the crack resistance of asphalt pavements in the study of technical standards for asphalt mixtures. In our country's "Seventh Five-Year" research project, some research studies have been carried out on the low-temperature performance of asphalt and asphalt mixture recommended value. There are many test methods to study the low-temperature performance of asphalt mixture, mainly including failure test with equal strain loading (indirect tensile test, bending test, compression test), direct tensile test, bending tensile creep test, restricted specimen temperature stress test, three-point bending J integral test, shrinkage coefficient test, and stress relaxation test. To better study the low-temperature crack resistance of semiflexible pavement materials, this study uses low-temperature bending test to test the low-temperature crack resistance of semiflexible pavement materials. The specimen was cured for 28 days under standard conditions, the test temperature was −10°C ± 0.5°C, the loading rate was 50 mm/min, and the specimen should be kept warm for at least 6 hours before the test (Figures 6 and 7). The specimens are maintained under standard conditions for 28 d at a test temperature of −10°C ± 0.5°C and a loading rate of 50 mm/min. The specimens are required to be insulated for at least 6 h before the test.

5. Results and Analyses

5.1. Compressive Strength and Deformation. Figure 8 shows the damaged form of prismatic specimens of different compressive strengths after the compressive test.

As can be seen from Figure 8, the compressive strengths of the specimen consist mainly of the embedding and internal frictional forces between the mineral particles and the cohesive force between the asphalt and the asphalt and minerals. When the axial pressure is applied, these forces gradually decrease and small cracks appear in the specimens. With the increase in pressure, the internal cracks develop rapidly and become several connected cracks, thus dividing

Figure 6: Insulating in the temperature test chamber.

Figure 7: Specimen after low-temperature insulation.

the specimen into several small blocks. When the external force exceeds the maximum compressive strength that the specimen can withstand, it is destabilized and stops working.

Comparing the data in Table 16, for the specimen of the SFP material at the same test age, when the strength of the cement mortar is 30.7 MPa, its compressive strength is 1.3 times that of the cement mortar strength of 19.8 MPa. When the strength of the cement mortar is 40.2 MPa, its compressive strength is 1.2 times that of the cement mortar strength of 30.7 MPa. With the increase in cement mortar strength, the compressive strength of cement grouting asphalt crushed stone material also increases. When the cement mortar strength is 40.2 MPa, the corresponding compressive strength is higher. With the increase in the test age, the compressive strength also increases, and the compressive strength is the highest at 28 d.

From the analysis of Figures 9 and 10, it can be seen that the test results of the two mixtures were evaluated by compressive tensile strength and compressive stiffness modulus, indicating that both mixtures showed good compressive performance. The curve shows a linear growth, indicating that the increase in grouting strength is positively correlated with the enhancement of compressive strength of SFP material. The compressive strength of composite materials is also different for different test ages. Among them, the compressive strength of 3 d, 7 d, and 28 d of test age increases gradually, and from the curve of stiffness modulus, the growth law of compressive stiffness modulus can be revealed. There is a certain similarity with the increase in compressive strength, which indicates that the compressive tensile strength and compressive stiffness modulus of SFP material increase with the increase in grouting material strength and test age.

5.2. Flexural and Tensile Resistance Tests. Figure 11 shows the damaged forms of prismatic specimens of different strengths after the beam bending test.

When asphalt macadam is damaged by bending, the cracks are mainly occurring along with the interface between the particles. The strength of the interface formed by the asphalt and mineral mixtures plays a decisive role in the bending and tensile properties of the specimen. With the mixing of cement slurry of appropriate amount into the matrix asphalt macadam, the strength of the interface formed by asphalt, minerals, and fibers is increased, enhancing the flexural and tensile strength of the asphalt concrete. The flexural and tensile strengths obtained through testing are shown in Table 17.

Comparing the data in Table 17, for the specimen of the SFP material at the same test age, when the strength of the cement mortar is 30.7 MPa, its flexural tensile strength is more than 1 times that of the cement mortar strength of 19.8 MPa. With the increase in cement mortar strength, the flexural tensile strength of cement grouting asphalt crushed stone material also increases. When the cement mortar strength is 40.2 MPa, the corresponding mechanical properties are stronger. As the age of the formed cement grouting asphalt macadam material increases, the flexural failure stiffness modulus also increases, which is also similar to the cement concrete material.

It can be seen from the analysis of Figures 12 and 13 that the test results of the two mixtures were evaluated by the flexural tensile strength and the flexural stiffness modulus, indicating that both mixtures showed good low-temperature crack resistance. The curve shows a linear growth, indicating that the increase in grouting strength is positively correlated with the enhancement of compressive strength of SFP material. From the bending stiffness modulus curve, it can be seen that the growth law of bending stiffness modulus has a certain similarity with the growth of bending tensile strength, which indicates that the bending tensile strength and bending stiffness modulus of SFP materials will increase with the grouting strength. The optimal bending tensile strength and bending stiffness modulus of SFP materials will occur at 40.2 MPa. The flexural tensile strength and flexural failure stiffness modulus of the formed cement grouting asphalt macadam material increase with the increase in age.

5.3. Compressive Resilient Modulus. The compressive resilient modulus of the asphalt macadam increases with the strength of the cement slurry, as shown in Table 18.

It can be learned from Table 18 that the compressive resilient modulus of asphalt macadam with cement slurry increases with the increase in cement slurry strength, but there is a higher compressive resilient modulus at low

(a) (b)

Figure 8: Damaged forms of the specimens. (a) Prismatic specimens before the test. (b) Specimens after the test.

Table 16: Uniaxial compressive test data processing results at the same cement slurry strength.

Cement slurry strength (MPa)	Test age (d)	Compressive strength R_c (MPa)	Compressive strain ϵ_c	The stiffness modulus in compression S_c (MPa)	Remarks
19.8	7	11.171	0.0363	307.612	Matrix asphalt macadam with a target porosity of 24%
	14	11.354	0.0354	321.226	
	28	11.850	0.0353	335.861	
30.7	7	13.674	0.0422	324.542	
	14	14.265	0.0394	362.355	
	28	15.010	0.0376	399.308	
40.2	7	16.641	0.0434	383.402	
	14	17.740	0.0423	419.482	
	28	18.509	0.0403	459.160	

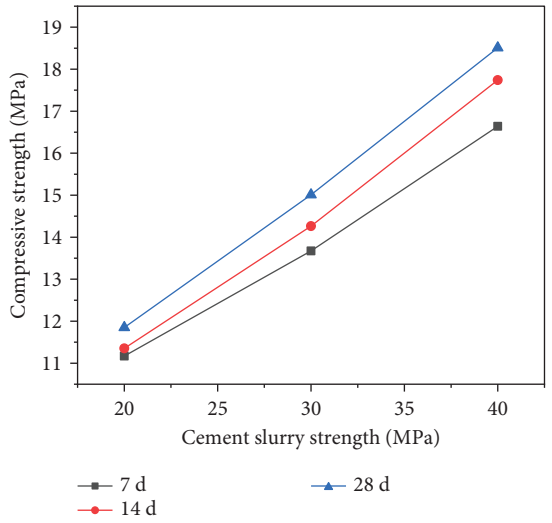

Figure 9: Variation curve of the compressive strength of the prismatic specimen with the strength of the cement slurry.

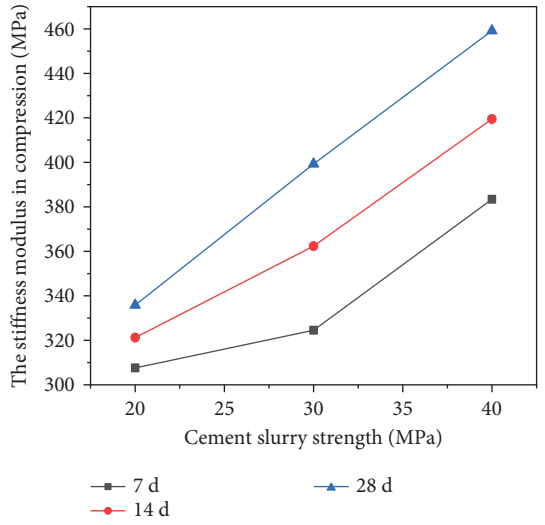

Figure 10: Variation curve of the stiffness modulus in compression with cement slurry strength.

temperatures. The strength of the cement slurry has the same effect on the change in compressive strength of both the cylinder and the prism, displaying a good linear relationship between both compressive strength and the cement slurry strength. The compressive resilient modulus of cement grouting asphalt macadam is 2800 MPa to 3600 MPa, which is generally higher than that of conventional asphalt concrete when the strength of the cement slurry ranges from 19.8 MPa to 40.2 MPa.

It can be seen from Figures 14 and 15 that the compressive strength at a temperature of 15°C is higher than that at a temperature of 20°C, indicating that the SFP material has better compressive strength at low temperature, and the curve shows a linear growth, indicating that the grouting strength is positively correlated with the compressive strength of the SFP material. From the compressive resilience modulus curve, it can be seen that the growth law of compressive resilience modulus has a certain similarity with the growth of compressive strength, which indicates that the compressive

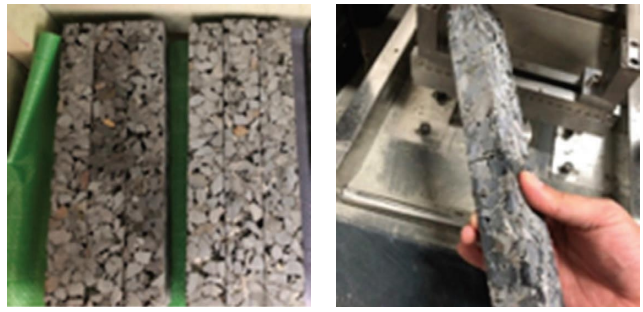

(a) (b)

Figure 11: Damaged specimens after the flexural and tensile test. (a) Prismatic specimens before the test. (b) The specimen after the test.

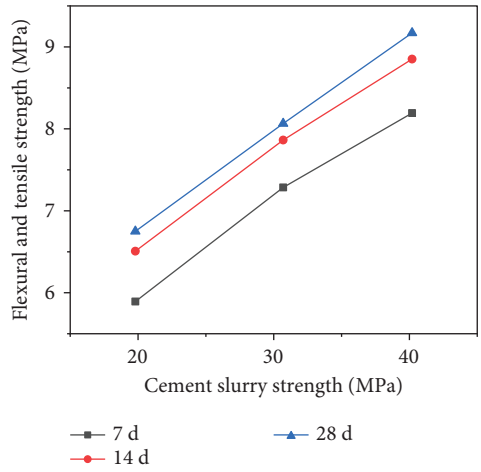

Figure 12: Variation curve of flexural tensile strength with cement slurry strength.

Table 17: Data processing results for beam bending tests at different cement slurry strengths.

Cement slurry strength (MPa)	Test age (d)	Flexural and tensile strength R_B (MPa)	Maximum flexural tensile strain ϵ_B	Modulus of flexural stiffness S_B (MPa)	Remarks
19.8	7	5.893	0.00176	3349.018	Matrix asphalt macadam with a target porosity of 24%
	14	6.507	0.00189	3440.938	
	28	6.750	0.00142	4763.936	
30.7	7	7.285	0.00154	4742.825	
	14	7.863	0.00162	4862.772	
	28	8.065	0.00161	5024.706	
40.2	7	8.193	0.00149	5498.589	
	14	8.852	0.00157	5652.827	
	28	9.171	0.00152	6049.540	

strength and compressive resilience modulus of SFP materials will increase with the increase in grouting strength and are optimal at 40.2 MPa.

5.4. High-Temperature Stability. Figure 16 shows the damaged forms of the specimen after the high-temperature stability test.

Compared with flexible asphalt macadam, the cement grouting asphalt mixture boasts better high-temperature dynamic stability. The main reason for this is that the matrix asphalt macadam is both rigid and flexible when filled with cement slurry in the large voids, and the cementitious material solidified at high temperatures forms a skeletal structure that restricts the flow of the matrix asphalt. As a result, the rutting depth is small, the dynamic stability is

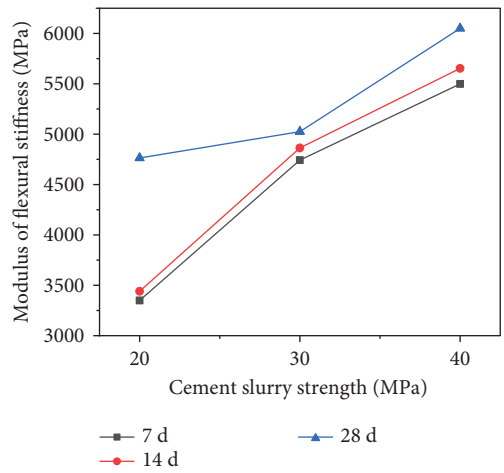

Figure 13: Variation curve of modulus of flexural stiffness with cement slurry strength.

Table 18: Data processing results of the rebound modulus test at different cement slurry strengths.

Cement slurry strength (MPa)	Compressive strength R_c (MPa)		Compressive resilient modulus E (MPa)		Remarks
	15°C	20°C	15°C	20°C	
19.8	9.93	9.41	3121.8	2869.2	
30.7	13.29	12.92	3525.6	3463.4	Matrix asphalt macadam with a target porosity of 24%
40.2	16.23	15.82	3757.2	3641.6	

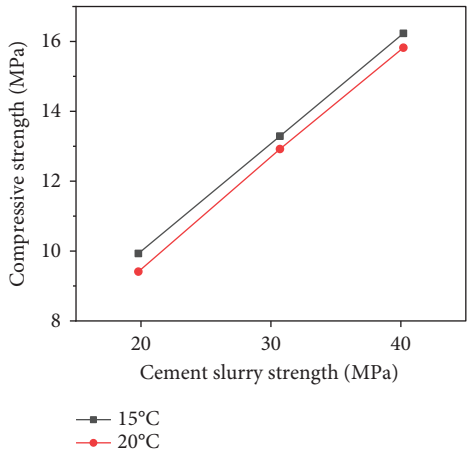

Figure 14: Variation curve of the compressive strength of the cylinder with the strength of the cement slurry.

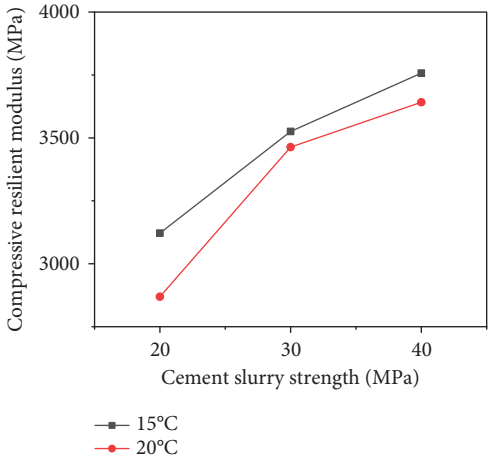

Figure 15: Variation curve of compressive resilient modulus with the cement slurry strength.

high, and the percentage reduction in dynamic stability affected by temperature changes is low.

As can be seen from Table 19, the test results of the two mixtures were evaluated by dynamic stability (DS) index, which showed that both mixtures exhibited good high-temperature stability. It can be found from Table 19 that the rut depth of the SFP material is very small, the rut depth is less than 1 cm, and the rut depth gradually decreases with the increase in the strength of the grouting material. The increase in the dynamic stability of the cement grouting asphalt crushed stone material will also increase with the increase in the strength of the cement mortar. When the pouring compressive strength is 40.2 MPa, the dynamic stability of the cement grouting asphalt crushed stone material reaches 63,000 times/mm. Even the cement mortar of 19.8 MPa and 30.7 MPa has a dynamic stability of more than 39,000 times/mm, which fully shows that the cement grouting asphalt crushed stone material has very good high-temperature stability.

From the dynamic stability curve shown in Figure 17, it can be seen that the growth slope of the dynamic stability curve of rutting when the grouting strength increases from 19.8 MPa to 30.7 MPa is lower than that when the grouting

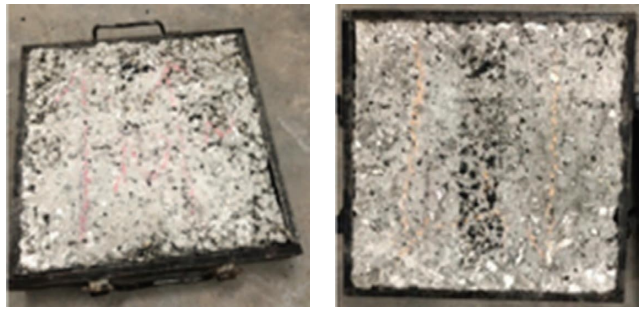

(a) (b)

Figure 16: Damaged forms of the specimen after the high-temperature test. (a) Rutting plates. (b) Rutting plate after the test.

Table 19: Data processing results of high-temperature stability tests at different cement slurry strengths.

Cement slurry strength (MPa)	D_1 (mm)	D_2 (mm)	Amount of deformation (mm)	Dynamic stability DS (times/mm)	Remarks
19.8	0.388	0.404	0.016	39375	Matrix asphalt macadam with a target porosity of 24%
30.7	0.342	0.356	0.014	45000	
40.2	0.254	0.262	0.008	63000	

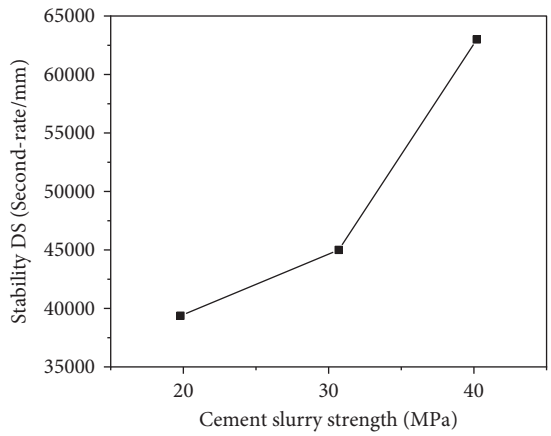

Figure 17: Variation curve of dynamic stability with cementitious mortar strength.

strength increases from 30.7 MPa to 40.2 MPa. The development of dynamic stability of asphalt crushed stone material develops slowly in the initial time and turns around when the strength of grouting material reaches 30.7 MPa. It can be known that the high-temperature stability of the SFP material can be considered to be very good whether it is from the perspective of dynamic stability or from the perspective of rutting depth. The high-temperature stability of asphalt mixture mainly refers to the ability of the material to resist shear flow deformation at high temperature. Due to the addition of cement in semiflexible materials, the rigidity of the material increases and the ability to resist shear flow deformation increases. The anti-rutting ability also increases.

5.5. Low-Temperature Crack Resistance. Asphalt mixtures do not differ considerably in low-temperature crack resistance. Due to the low content of structural asphalt and poor adhesion between the asphalt binders and the mineral materials, the asphalt mixture tends to spall easily at low temperatures, which reduces its resistance to temperature stress, and hence, damages occur. The infusion of cement slurry, however, can change this situation to a large extent. The experimental data are shown in Table 20.

It can be learned from Table 20 that similar to the results of the beam bending test at 15°C, the flexural and tensile strength and the modulus of flexural stiffness of the cement grouting asphalt macadam at −10°C also increase with the increase in cement slurry strength, while its flexural tensile strength at low temperatures is even lower, and this change can be more intuitively seen in Figures 18 and 19. The maximum flexural strain at low temperatures decreases with the increase in cement slurry strength, so it is possible to increase the deflection of the cement grouting asphalt macadam at low temperatures by appropriately reducing the strength of the cement slurry to prevent brittle damage at low temperatures while maintaining its mechanical properties.

Table 20: Data processing results of low-temperature beam bending tests at different cement slurry strengths.

Cement slurry strength (MPa)	Flexural and tensile strength R_f (MPa)	Maximum flexural and tensile strain ϵ_R	Modulus of flexural stiffness S_R (MPa)	Remarks
19.8	5.851	0.00108	5397.843	Matrix asphalt macadam with a target porosity of 24%
30.7	7.389	0.000976	7571.118	
40.2	7.954	0.000882	9018.509	

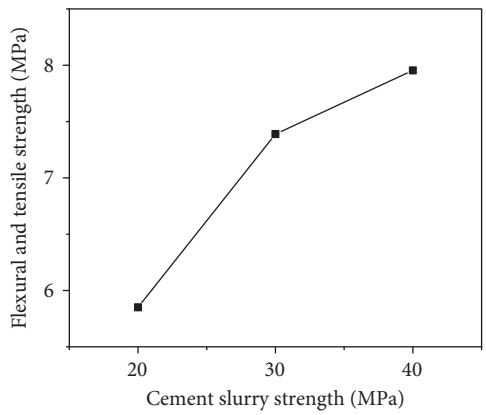

Figure 18: Variation curve of flexural and tensile strength with the cement slurry strength at −15°C.

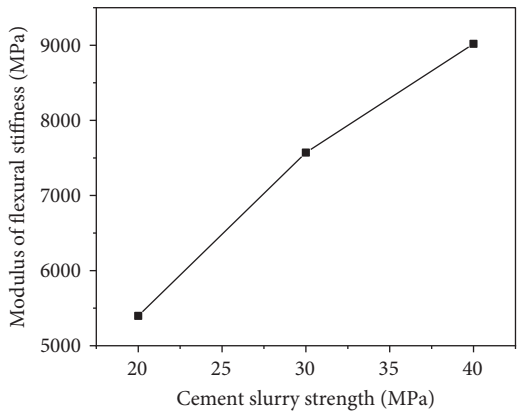

Figure 19: Variation curve of modulus of flexural stiffness with the cement slurry strength at −15°C.

6. Conclusion

In this study, the effect of cement slurry strength on the performance of cement grouting asphalt macadam materials (semiflexible pavement materials) is investigated. In terms of mechanical properties, the compressive strength and flexural and tensile strength of SFP materials and the compressive resilient modulus are measured; in terms of road performance, high-temperature stability and low-temperature crack resistance of SFP materials are investigated. The conclusions can be listed as follows:

(1) The combination of cement mortar and porous asphalt gravel greatly improves the strength of porous asphalt gravel. In addition, the strength of cement mortar is an important factor affecting the performance of SFP materials.

(2) The compressive test results show that the compressive strength of the SFP material increases with age, and the compressive strength and elastic modulus increase with the increase in the strength of the grouting material. When the test age is 28 d, the grouting material with a strength of 30.7 MPa has a 28 d compressive strength increased by 27% compared with the strength of the grouting material of 19.8 MPa. Compared with the grouting material at the strength of 30.7 MPa, the grouting material at the strength of 40.2 Mpa witnesses a 23% increase in the 28-day compressive strength. Compared with 30.7 MPa, the 28-day compressive strength of SFP material increased by 23%. When the experimental temperature is 15°C, the grouting material with a strength of 30.7 MPa has a 13% increase in the compressive modulus of resilience compared with the grouting material with a strength of 19.8 MPa. When the grouting material strength is 40.2 MPa, compared with 30.7 MPa, the compressive resilience modulus is increased by 7%.

(3) The results of Marshall test and rutting test show that the SFP material mixed with grouting material exhibits good high-temperature stability, and the dynamic stability increases with the increase in the strength of the grouting material. Compared with the grouting material at the strength of 19.8 MPa, the grouting material at the strength of 30.7 Mpa witnesses a 14% increase in the dynamic stability. When the strength of the grouting material is 40.2 MPa, the dynamic stability of the SFP material is increased by 40% compared with the strength of the grouting material of 30.7 MPa.

(4) The results of the trabecular bending test show that the SFP material mixed with the grouting material exhibits good low-temperature crack resistance and flexural tensile strength. The low-temperature flexural tensile strength increases with the increase in the grouting material strength. The 30.7 MPa grouting material has a 26% increase in the low-temperature bending tensile strength compared with the 19.8 MPa grouting material strength. When the grouting material strength is 40.2 MPa, compared with the grouting material strength of 30.7 MPa, the low-temperature bending tensile strength has an 8% increase.

It can be seen that the SFP material prepared from cement slurry with large void matrix asphalt macadam displays improved mechanical properties and can better meet durability requirements related to pavement

performance. Cement slurry infusion can significantly improve the compressive strength of the material and contributes to even better mechanical properties when the grouting material strength is 40.2 MPa.

Data Availability

The data used to support the findings of this study are available from the corresponding author upon request.

Conflicts of Interest

The authors declare that they have no conflicts of interest regarding the publication of this study.

Acknowledgments

The authors acknowledge China Railway 24th Bureau Group Xinyu Engineering Co. Ltd for providing financial support.

References

[1] S. Zhang, Y. He, H. Zhang, J. Chen, and L. Liu, "Effect of fine sand powder on the rheological properties of one-part alkali-activated slag semi-flexible pavement grouting materials," *Construction and Building Materials*, vol. 333, Article ID 127328, 2022.

[2] J. Yajun and J. H. Cahyadi, "Effects of densified silica fume on microstructure and compressive strength of blended cement pastes," *Cement and Concrete Research*, vol. 33, no. 10, pp. 1543–1548, 2003.

[3] Y. Fang, X. Wang, L. Jia et al., "Synergistic effect of polycarboxylate superplasticizer and silica fume on early properties of early high strength grouting material for semi-flexible pavement," *Construction and Building Materials*, vol. 319, Article ID 126065, 2022.

[4] A. Costas, "Anagnostopoulos, Effect of different superplasticizers on the physical and mechanical properties of cement grouts," *Construction and Building Materials*, vol. 50, pp. 162–168, 2014.

[5] D. Rezazadeh Eidgahee, H. Jahangir, N. Solatifar, P. Fakharian, and M. Rezaeemanesh, "Data-driven estimation models of asphalt mixtures dynamic modulus using ANN, GP and combinatorial GMDH approaches," *Neural Computing & Applications*, vol. 34, no. 20, pp. 17289–17314, 2022.

[6] S. Wang, H. Zhou, X. Chen, M. Gong, J. Hong, and X. Shi, "Fatigue resistance and cracking mechanism of semi-flexible pavement mixture," *Materials*, vol. 14, no. 18, p. 5277, 2021.

[7] S. Hou, T. Xu, and K. Huang, "Investigation into engineering properties and strength mechanism of grouted macadam composite materials," *International Journal of Pavement Engineering*, vol. 17, no. 10, pp. 878–886, 2016.

[8] Q. J. Ding, Z. Sun, F. Shen, and S. L. Huang, "The performance analysis of semi-flexible Pavement by the volume parameter of matrix asphalt mixture," *Advanced Materials Research*, vol. 168-170, pp. 351–356, 2010.

[9] W. Zhao and Q. Yang, "Study on the applicability of asphalt concrete skeleton in the semi-flexible pavement," *Construction and Building Materials*, vol. 327, Article ID 126923, 2022.

[10] B. Yang and X. Weng, "The influence on the durability of semi-flexible airport pavement materials to cyclic wheel load testfluence on the durability of semi-flexible airportpavement materials to cyclic wheel load test," *Construction and Building Materials*, vol. 98, pp. 171–175, 2015.

[11] N. M. Husain, M. R. Karim, H. B. Mahmud, and S. Koting, "Effects of aggregate gradation on the physical properties of semiflexible pflexible pavement," *Advances in Materials Science and Engineering*, vol. 2014, Article ID 529305, 8 pages, 2014.

[12] S. Ling, M. Hu, D. Sun, H. Ni, and L. Xu, "Mechanical properties of pouring semi-flexible pavement material and engineering estimation on contribution of each phase," *Construction and Building Materials*, vol. 315, Article ID 125782, 2022.

[13] H. Jahangir, A. Soleymani, and M. R. Esfahani, "Investigating the confining effect of steel reinforced polymer and grout composites on compressive behavior of square concrete columns," *Iranian Journal of Science and Technology, Transactions of Civil Engineering*, vol. 11, pp. 1–17, 2022.

[14] S. Koting, M. Karim, H. Mahmud, and N. Hamid, "Development of cement-bitumen composites for semi-flexible pavement surfacing," *Proceedings of the Eastern Asia Society for Transportation Studies*, vol. 8, 2011.

[15] J. Pei, J. Cai, D. Zou et al., "Design and performance validation of high-performance cement paste as a grouting material for semi-flexible pavement," *Construction and Building Materials*, vol. 126, pp. 206–217, 2016.

[16] J. Zhang, J. Cai, J. Pei, R. Li, and X. Chen, "Formulation and performance comparison of grouting materials for semi-flexible pavement," *Construction and Building Materials*, vol. 115, pp. 582–592, 2016.

[17] M. L. Afonso, M. Dinis-Almeida, L. A. Pereira-de-Oliveira, J. Castro-Gomes, and S. E. Zoorob, "Development of a semi-flexible heavy duty pavement surfacing incorporating recycled and waste aggregates-preliminary study," *Construction and Building Materials*, vol. 102, pp. 155–161, 2016.

[18] A. Solouki, P. Tataranni, and C. Sangiorgi, "Thermally treated waste silt as geopolymer grouting material and filler for semiflexible pavements," *Infrastructure*, vol. 7, no. 8, p. 99, 2022.

[19] M. Hamzani, M. Hasan, M. Hasan, and S. Sugiarto, "Determining the properties of semi-flexible pavement using waste tire rubber powder and natural zeolite," *Construction and Building Materials*, vol. 266, Article ID 121199, 2021.

[20] M. Hamzani, M. Hasan, M. Hasan, Z. Zulfhazli, and Zulfhazli, "Permanent deformation and fatigue of semi flexible pavement incorporating waste tire rubber and natural zeolite," *Key Engineering Materials*, vol. 892, pp. 51–58, 2021.

[21] M. Hamzani, M. Hasan, M. Hasan, and S. Sugiarto, "The influence of the using waste tire rubber and natural ziolite as Asphalt and Cement replacements to compressive strength of Semi-Flexible Pavement," *IOP Conference Series: Materials Science and Engineering*, vol. 523, no. 1, Article ID 012037, 2019.

[22] J. Cai, J. Pei, Q. Luo, J. Zhang, R. Li, and X. Chen, "Comprehensive service properties evaluation of composite grouting materials with high-performance cement paste for semi-flexible pavement," *Construction and Building Materials*, vol. 153, pp. 544–556, 2017.

[23] X. Cai, W. Huang, and K. Wu, "Study of the self-healing performance of semi-flexible pavement materials grouted with engineered cementitious composites mortar based on a non-standard test," *Materials*, vol. 12, no. 21, p. 3488, 2019.

[24] X. Liang, X. Zou, W. Wu, and W. Wu, "Critical appraisal on pavement performance of early-strength irrigated semi-

flexible pavement," *AIP Conference Proceedings*, vol. 2154, no. 1, 2019.

[25] D. Wang, X. Liang, C. Jiang, and Y. Pan, "Impact analysis of Carboxyl Latex on the performance of semi-flexible pavement using warm-mix technology," *Construction and Building Materials*, vol. 179, pp. 566–575, 2018.

[26] J. Hong, K. Wang, Z. Xiong et al., "Investigation into the freeze–thaw durability of semi-flexible pavement mixtures," *Road Materials and Pavement Design*, vol. 21, no. 8, pp. 2198–2214, 2019.

[27] J. Ren, Y. Xu, Z. Zhao et al., "Fatigue prediction of semi-flexible composite mixture based on damage evolution," *Construction and Building Materials*, vol. 318, Article ID 126004, 2022.

[28] B. Fang, T. Xu, and S. Shi, "Laboratory study on cement slurry formulation and its strength mechanism for semi-flexible pavement," *Journal of Testing and Evaluation*, vol. 44, no. 2, Article ID 20150230, 2016.

[29] M. Imran Khan and M. Hartadi Sutanto, "Irradiated polyethylene terephthalate and fly ash based grouts for semi-flexible pavement: design and optimisation using response surface methodology," *International Journal of Pavement Engineering*, vol. 186, 2020.

[30] H. Tan, Z. Xiong, M. Gong, J. Chen, J. Hong, and Č. Robert, "Investigation on the influences of curing time on the cracking resistance of semiflexible pavement mixture," *Advances in Materials Science and Engineering*, vol. 2021, Article ID 8855565, 15 pages, 2021.

[31] Jtg, *Test Specification for Cement and concrete in Highway Engineering*, 2005.

[32] *General Portland Cement*, 2005.

[33] S. Ya-zhen, C. Yuan-yuan, D. Min, and S. Chao-zhuo, "Design and performance of semi-flexible pavement materials," *Concrete*, vol. 9, pp. 124–131, 2019.

[34] W. Wei, H. Huiming, and W. Ruxi, *Journal of highway and transportation science and technology*, vol. 34, no. 5, pp. 35–41, 2017.

[35] F. Qin, "Study on the performance of semiflexible pavement pouring composite mortar," *Concrete*, vol. 6, pp. 97–102, 2016.

[36] C. Xiangfeng, *Mixture Design of High Performance Fluid Cement Grouting Materials and Pavement Performance of Semi-flexible Pavement*, Chang 'an University, Chang, 2010.

[37] L. Cheng, *Research on Properties and Design Methods of Mixtures for Semi-flexible Pavement*, Chang'an University, Chang, 2002.